RSC Advances

PAPER

View Article Online
View Journal | View Issue

Check for updates

Cite this: *RSC Adv.*, 2025, **15**, 6774

Cellulose aerogel-based copper oxide/carbon composite for supercapacitor electrode†

Yu Qian, Xinye Sun, Xinyue Deng, Shiqin Yin and Tao Zhang *

Carbon composite is one of the most competitive electrode materials for supercapacitor, and improving its energy density remains a significant challenge. The copper oxide/carbon composites with high specific surface area were prepared from the cellulose aerogel loaded with copper salts. The copper oxide/carbon composite electrode material, deriving from copper sulfate, reached a specific capacitance of 1001 F g^{-1} at 2 A g^{-1}, with an energy density of 139.0 W h kg^{-1}. After 500 cycles, the capacitance retention rate is 98.06%. An asymmetric supercapacitor was assembled using this material as positive electrode material, activated carbon as negative electrode material, and 3.0 M KOH as electrolyte. It exhibited good reversible capacity and low voltage drop loss within a voltage window of 0–1.2 V, and its specific capacitance and energy density achieved 125 F g^{-1} and 6.3 W h kg^{-1} at a current density of 0.1 A g^{-1}, respectively.

Received 31st December 2024
Accepted 20th February 2025

DOI: 10.1039/d4ra09119a

rsc.li/rsc-advances

Open Access Article. Published on 03 March 2025. Downloaded on 6/14/2026 4:03:39 PM.
This article is licensed under a Creative Commons Attribution-NonCommercial 3.0 Unported Licence.

1 Introduction

Supercapacitors, as important electrochemical energy storage devices, offer advantages such as high power density and long cycle life. An energy storage system that combines supercapacitors with batteries is considered a safe and efficient solution to the problem of unstable power supply from some new energy sources, like wind and solar energy.[1,2]

At present, the challenge limiting the further application of supercapacitors is their relatively low energy density, and improving electrode material is crucial to solving this problem.[3,4] Based on the high specific surface area, carbon materials are the typically main component of the electrode,[5] which includes activated carbon,[6,7] graphene,[8,9] carbon nanotubes,[10,11] and carbon aerogels.[12,13] Zhu *et al.* employed potassium hydroxide to activate exfoliated graphite oxide, resulting in a porous carbon material with a high specific surface area of 3100 m^2 g^{-1}, and the specific capacitance could reach 200 F g^{-1} in the [EMIM]TFSI electrolyte.[14] Wang *et al.* treated the carbon nanotubes (CNTs) with alkali and mixed acids to improve their specific surface area and the pore distribution.[15] The specific capacitance of the treated CNTs achieved 85 F g^{-1} in H_2SO_4 electrolyte, which was 3 times higher than that of raw CNTs. Lei *et al.* prepared carbon aerogel by using cellulose aerogel as a precursor, which was obtained by dissolving microcrystalline cellulose into a NaOH–urea–H_2O mixed solution. With a three-dimensional porous network structure and a high specific surface area of 1130 m^2 g^{-1}, the specific capacitance of the carbon aerogel could reach 106.2 F g^{-1} at 1 mA cm^{-2}.[16]

Based on the energy storage mechanism, pure carbon materials are double-layer capacitors and their specific capacitance are generally limited. In order to enhance the energy density, pseudocapacitive electrode materials, such as transition metal oxides,[17,18] transition metal sulfides,[19,20] and metal–organic frameworks (MOFs),[21,22] are combined with carbon materials to utilize their faradaic reactions to increase the specific capacitance of the electrodes. Naderi *et al.* used high-intensity ultrasound radiation to uniformly dispersed the MnO_2 particles on the nitrogen-doped reduced graphene, and the specific capacitance of this composite reached 522 F g^{-1} at 2 mV s^{-1}.[23] As bimetallic sulfide, the $NiCo_2S_4$ nanomaterial was deposited on the reduced graphene oxide to fabricate electrode composite, which could exhibit a high specific capacitance of 1242.2 F g^{-1} at a current density of 1 A g^{-1}.[24] Wen *et al.* synthesized Ni-MOF/CNTs composites by solvothermal method.[25] The specific capacitance reached 1765 F g^{-1} at a current density of 0.5 A g^{-1}. The excellent performance could be attributed to the synergistic effects of Ni-MOF and CNTs, including the porous nanostructure of the Ni-MOF and the high electronic conductivity of CNTs. In addition to metal-related pseudocapacitance, the combination of conductive polymers such as polyacetylene, polyaniline, polypyrrole with carbon materials also shows potential in the field of supercapacitor electrode materials.[26,27]

Cellulose aerogel is considered an ideal precursor for carbon electrode materials, which can form carbon materials with a large specific surface area after carbonization.[28,29] Moreover, composite materials formed by cellulose carbon aerogel and metal oxides such as GeO_2, Fe_3O_4 and Co_3O_4 have demonstrated

School of Chemical Engineering, Sichuan University, Chengdu 610065, China. E-mail: zhangtao@scu.edu.cn

† Electronic supplementary information (ESI) available. See DOI: https://doi.org/10.1039/d4ra09119a

© 2025 The Author(s). Published by the Royal Society of Chemistry

Open Access Article. Published on 03 March 2025. Downloaded on 6/14/2026 4:03:39 PM. This article is licensed under a Creative Commons Attribution-NonCommercial 3.0 Unported Licence.

excellent electrochemical performance.[30,31] In this work, cellulose aerogel was prepared by dissolving cellulose in ionic liquids, and copper(II) acetate ($Cu(OAc)_2$), copper(II) nitrate trihydrate ($Cu(NO_3)_2$), and copper(II) sulfate pentahydrate ($CuSO_4$) were loaded onto the cellulose aerogel, respectively. After carbonization, copper oxide/carbon composite electrode materials were obtained, combining the large specific surface area of carbon materials and the pseudocapacitive characteristics of copper oxides to enhance the materials' specific capacitance. The electrochemical performance of the copper oxide/carbon materials was studied through cyclic voltammetry, constant current charge–discharge, electrochemical impedance spectroscopy, and cycling stability tests in a three-electrode system. The electrochemical principles of the copper oxide/carbon materials were analyzed using X-ray diffraction, Raman spectroscopy, scanning electron microscopy, and X-ray photoelectron spectroscopy.

2 Experimental section

2.1 Materials and reagents

The cellulose material (refined cotton) was provide by Tianpu Chemicals Co., Ltd. Dilute hydrochloric acid (AR), acetone (AR), $Cu(OAc)_2$ (>98%), $Cu(NO_3)_2 \cdot 3H_2O$ (AR), $CuSO_4 \cdot 5H_2O$ (AR), and potassium hydroxide (AR) were purchased from Chengdu Kelon Chemical Co., Ltd. 1-Allyl-3-methylimidazolium chloride ([AMIM]Cl) was supplied by Lanzhou Institute of Chemical Physics. Foam nickel (350 g m^{-2}), acetylene black (99.9%) and polyvinylidene fluoride (PVDF) powder were all purchased from Cyber Electrochemical Materials Network. Activated carbon (98%) was provided by Poersi Carbon Material Technology Co., Ltd. *N*-Methyl-2-pyrrolidone (AR) was purchased from Chengdu Zhuopu Instrument Co., Ltd.

2.2 Preparation of cellulose aerogels

Weigh 0.40 g of cotton cellulose and add 19.60 g of [AMIM]Cl into a three-necked flask. Under a nitrogen atmosphere, stir the mixture at 120 °C in an oil bath for 2 hours to form a homogeneous cellulose solution. Immediately pour the solution into a container and ultrasonicate for 1 hour to remove air bubbles, then place the solution at −5 °C for 2 hours to generate a sol. Immerse the gel into ultrapure water to remove the 1-allyl-3-methylimidazolium chloride, and then use 100 mL of *tert*-butanol as the replacement solvent, changing it every 8 hours for a total of two times, to obtain a cellulose gel. Freeze this gel in liquid nitrogen for 10 minutes, and then subject it to vacuum freeze-drying at −56 °C for 24 hours to prepare the cellulose aerogel.

2.3 Preparation of copper oxide/carbon composite

Add 1.00 g of crushed cellulose aerogel in a flask with 50 mL water–ethanol mixed solution (volume ratio of 1 : 1). According to a copper-to-aerogel mass ratio of 4%, add $Cu(OAc)_2$, $Cu(NO_3)_2$ and $CuSO_4$ solutions with a concentration of 0.1 mol L^{-1}, respectively. Stir for 1 hour, then place the mixture in a rotary evaporator and evaporate at 50 °C. Afterward, dry the product in an oven at 60 °C to obtain cellulose aerogels loaded with copper salts as the precursors, denoted as CuO_x/A, CuO_x-N/A, and CuO_x-S/A. Place the precursors in a tubular furnace and heat them to 850 °C under an argon atmosphere for 2 hours to obtain copper oxide/carbon composites, denoted as CuO_x/CA, CuO_x-N/CA, and CuO_x-S/CA.

2.4 Material characterization

The specific surface area, pore volume, and pore size of the electrode materials were determined by the N_2 BET method with a Micromeritics ASAP 2420 fully automatic surface area and pore size analyzer. The morphology and pore structure of the copper oxide/carbon composite materials were observed using a JSM 7610F scanning electron microscope. The crystalline structure of copper oxide in the copper oxide/carbon composite materials was analyzed using an XD3 type X-ray diffractometer. The LabRAM HR Evolution type laser Raman spectrometer was used to analyze the degree of material defects. The presence of elements in the materials was characterized by the Escalab 250xi type X-ray photoelectron spectrometer.

2.5 Electrochemical measurement

The copper oxide/carbon electrode material was mixed with acetylene black and polyvinylidene fluoride (PVDF) in a ratio of 8 : 1 : 1 in an agate mortar and pestle for 30 minutes, and then *N*-methyl-2-pyrrolidone was added dropwise to achieve a uniform mixture. This mixture was coated onto foam nickel that had been treated with dilute hydrochloric acid, acetone, and deionized water, with dimensions of 1 × 1 cm^2. The coated foam nickel was then placed in an oven at 60 °C for 12 hours to dry, followed by calendering at 10 MPa for 5 minutes to fabricate the electrodes. A three-electrode system was assembled with 3.0 M KOH as the electrolyte, Hg/HgO as the reference electrode, and a platinum plate electrode as the counter electrode. The electrode material was immersed in the electrolyte for 12 hours prior to testing to ensure stability. The two-electrode system employed a coin cell (CR2025) configuration of an asymmetric supercapacitor, with CuO_x-S/CA as the positive electrode material, activated carbon as the negative electrode material and foam nickel as current collector. The assembly was carried out in sequence with the positive electrode shell, positive electrode plate, cellulose separator, negative electrode plate, stainless-steel spacer, spring, and negative electrode shell. After adding 3.0 M KOH as the electrolyte, the cell was encapsulated under 10 MPa and left for two hours before testing. The electrochemical performance of the electrode material was analyzed using a CHI760E electrochemical workstation, including cyclic voltammetry (CV), galvanostatic charge–discharge tests (GCD), electrochemical impedance spectroscopy (EIS), and cycling performance tests. The mass-specific capacitance, energy density, and power density of the electrode material were calculated using eqn (1) and (2).

$$C_m = \frac{I\Delta t}{m\Delta v} \quad (1)$$

Open Access Article. Published on 03 March 2025. Downloaded on 6/14/2026 4:03:39 PM. This article is licensed under a Creative Commons Attribution-NonCommercial 3.0 Unported Licence.

$$E = \frac{1}{2} C_m V^2 \quad (2)$$

In these equations, C_m represents the mass-specific capacitance of the electrode material (F g^{-1}), I represents the discharge current (A), Δt is the change in discharge time (s), m represents the mass of the active material on the working electrode (g), Δv represents the discharge voltage (V), E is the energy density of the supercapacitor W h kg^{-1}, V denotes the voltage range of the supercapacitor (V).

3 Results and discussion

3.1 Electrochemical performance analysis

The cyclic voltammetry curves of three oxide/carbon composites electrodes are shown in Fig. 1. Within the lower scanning rate range of 5–50 mV s^{-1}, a pair of redox peaks appear at −0.29 V in the CV curves of all three electrodes, which was mainly due to the valence change of the copper oxide. Within the higher scanning rate range of 75–125 mV s^{-1}, the redox peaks in the CV curves are diminished. As the scan rate increases, the redox peaks characterizing pseudocapacitance gradually weaken, while the rectangular features of electric double-layer capacitance (EDLC) become more pronounced, indicating a significant decrease in the ratio of pseudocapacitance to EDLC. This can be attributed to the rate limitation of the copper oxide redox reactions, which proceed more completely at lower scan rates, providing larger pseudocapacitance capacity, but fail to fully proceed at higher scan rates, reducing pseudocapacitance capacity.

At the current density range of 2–20 A g^{-1}, the GCD curves for the three electrodes were measured, as shown in Fig. 2(a)–(c). Compared to the ideal double-layer curves, these results exhibit varying degrees of deformation, with the nonlinear regions indicating the pseudocapacitive characteristics of the materials.[32] At a current density of 2 A g^{-1}, the GCD curves for CuO_x/CA, CuO_x-N/CA, and CuO_x-S/CA exhibit charge–discharge times of 278.4 s, 253.5 s, and 1032.8 s, respectively. The specific capacitances are calculated to be 254 F g^{-1}, 239 F g^{-1}, and 1001 F g^{-1}, respectively, and the energy densities are 33.3 W h kg^{-1}, 35.3 W h kg^{-1}, and 139.0 W h kg^{-1}, respectively. Fig. S1 and Table 1 in ESI †document illustrate the electrochemical properties of the pure cellulose carbon aerogel without copper salts or copper oxides. The specific capacitance and the energy density of the cellulose carbon aerogel are calculated to be 61 F g^{-1} and 8.5 W h kg^{-1}, respectively. These results suggest that using cellulose aerogel loaded with copper sulfate as a precursor is a superior method for preparing copper oxide/carbon composite materials. Compared to pure cellulose carbon aerogel, this composite material shows significant improvements in both specific capacitance and energy density. The GCD curve of CuO_x-N/CA shows shorter platform regions at voltages of −0.29 V and −0.70 V, corresponding to the valence transition of Cu(II) to Cu(I) and then to Cu(0). The GCD curve of CuO_x-S/CA exhibits a relatively long platform region at a voltage of −0.70 V, also corresponding to the redox reaction during the transition from Cu(I) to Cu(0).[33] Additionally, as shown in Fig. 2(d), the electrode resistances for CuO_x/CA, CuO_x-N/CA, and CuO_x-S/CA are 0.96 Ω, 1.01 Ω, and 1.10 Ω, respectively, all exhibiting relatively low resistance values.

Cyclic stability test was conducted on CuO_x-S/CA, which has the highest specific capacitance among the three composites mentioned above. As shown in Fig. 3, the result indicates that the specific capacity of this material can remain essentially unchanged after 500 cycles, with a retention rate of 98.06%.

Using CuO_x-S/CA as the positive electrode material and activated carbon as the negative electrode material, the asymmetric supercapacitor was assembled, and the cyclic voltammetry curves for different voltage intervals were determined at a scan rate of 2 mV s^{-1}. As shown in Fig. 4, with voltage windows of 0–1.0 V and 0–1.2 V, the cyclic voltammetry curves maintain similar rectangular shapes. When the voltage window is expanded to 0–1.3 V, the shape of the CV curve is deformed, and it exhibits a lower coulombic efficiency. Therefore, the voltage range for electrochemical performance testing is set to 0–1.2 V.

Fig. 5 displays the electrochemical performance tests of the assembled asymmetric supercapacitor with a voltage window of 0–1.2 V. As shown in Fig. 5(a), the CV curves at scan rates from 2 to 50 mV s^{-1} all exhibit similar rectangular shapes, and the enclosed area gradually increases with the increase in scan rate. Fig. 5(b) illustrates all GCD curves from 0.1 to 1.0 A g^{-1} display highly linear symmetrical triangular shapes. At 1.0 A g^{-1}, the curve exhibits a voltage drop of approximately 0.08 V, indicating good reversibility. Fig. 5(c) presents the AC impedance spectrum of the asymmetric supercapacitor. The Nyquist plot consists of a standard semicircle in the high-frequency region

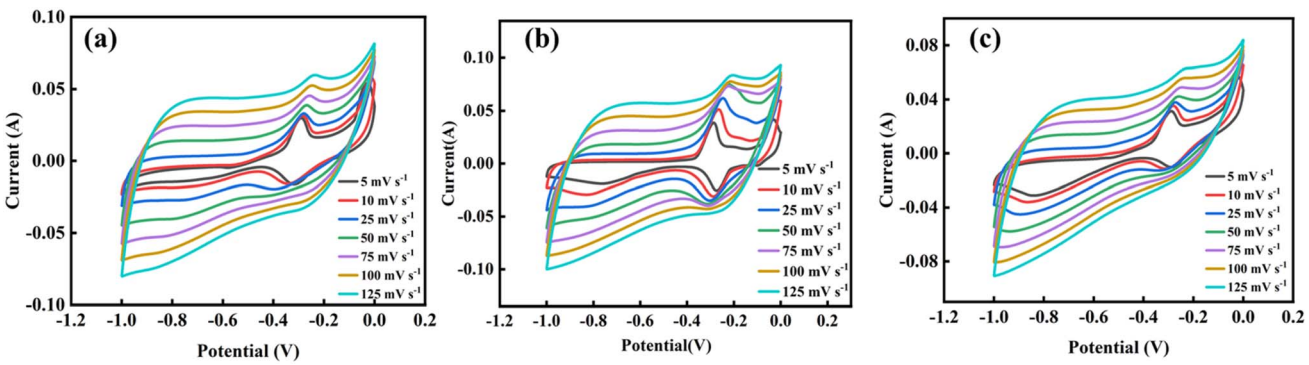

Fig. 1 Cyclic voltammetry curves of copper oxide/carbon composite electrode materials (a) CuO_x/CA, (b) CuO_x-N/CA, (c) CuO_x-S/CA.

© 2025 The Author(s). Published by the Royal Society of Chemistry

Open Access Article. Published on 03 March 2025. Downloaded on 6/14/2026 4:03:39 PM.
This article is licensed under a Creative Commons Attribution-NonCommercial 3.0 Unported Licence.

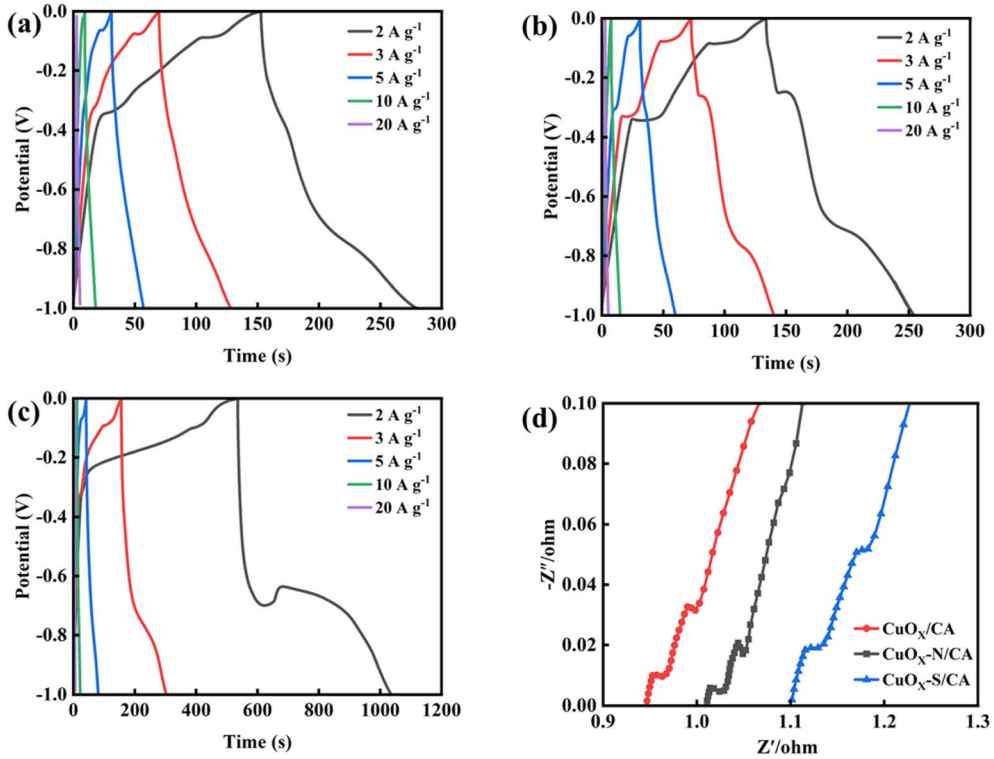

Fig. 2 Galvanostatic charge/discharge curve of copper oxide/carbon composite electrode materials. (a) CuO_x/CA, (b) CuO_x-N/CA, (c) CuO_x-S/CA, (d) AC impedance curve.

Table 1 The BET results of CuO_x/CA, CuO_x-N/CA, CuO_x-S/CA and their precursors

Sample	S_{BET} ($m^2\ g^{-1}$)	Pore volume ($cm^3\ g^{-1}$)	Average pore size (nm)
CuO_x/A	135	0.32	11.26
CuO_x-N/A	189	0.51	11.70
CuO_x-S/A	191	0.57	11.36
CuO_x/CA	264	0.08	2.94
CuO_x-N/CA	311	0.12	3.06
CuO_x-S/CA	394	0.47	5.12

and a straight line in the low-frequency region. The fixed resistance of the electrode is only 0.60 Ω, and the charge transfer resistance during charging and discharging is approximately 8.65 Ω. As shown in Fig. 5(d), at a current density of 1.0 A g^{-1}, the capacity retention after 1000 cycles is about 60%.

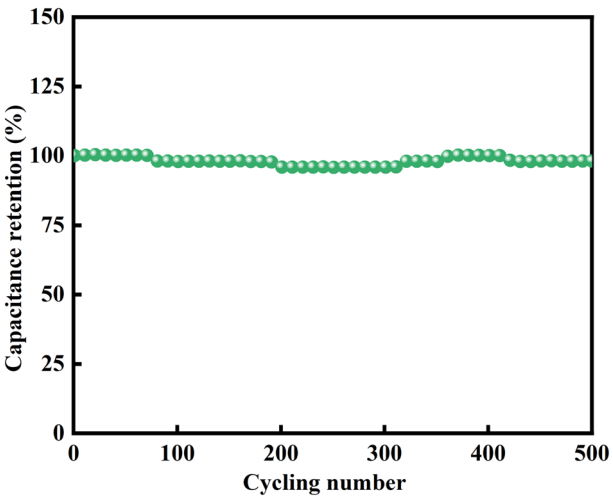

Fig. 3 Cyclic performance diagram of 2 A g^{-1} of CuO_x-S/CA.

3.2 Material characterization

3.2.1 BET analysis. The nitrogen adsorption–desorption isotherms for the copper oxide/carbon composites and their copper salt/cellulose aerogel precursors are shown in Fig. 6. All samples exhibit type IV isotherm adsorption curves, indicating the presence of a large number of micropores and mesopores in these materials, which is beneficial for the transport and storage of the electrolyte.

The specific surface area, pore volume, and pore size of these materials are presented in Table 1. Compared to the precursors, the specific surface areas of the copper oxides/carbon composites have significantly increased. The CuO_x-S/CA has the largest specific area of 394 $m^2\ g^{-1}$, which is consistent with its higher specific capacitance and energy density relative to CuO_x/CA and CuO_x-N/CA. In addition, the average pore size of the materials after carbonization has been significantly reduced, and the proportion of micropores has greatly increased. As shown in Table S2 in ESI† document, the specific surface areas of cellulose aerogel and cellulose carbon aerogel are 289 and 291 m^2

Open Access Article. Published on 03 March 2025. Downloaded on 6/14/2026 4:03:39 PM.
This article is licensed under a Creative Commons Attribution-NonCommercial 3.0 Unported Licence.

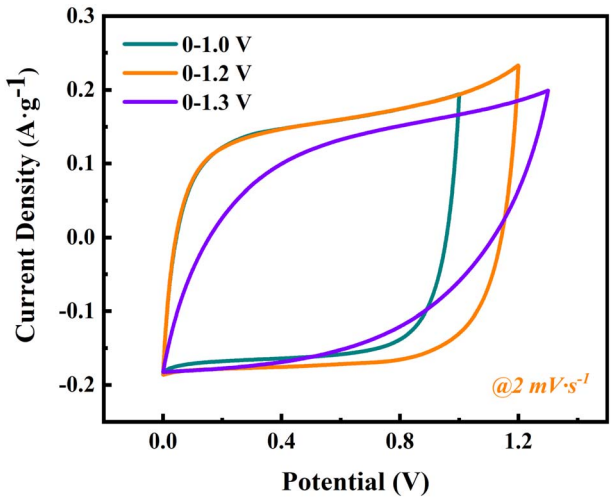

Fig. 4 Cyclic voltammetry curves for different voltage ranges.

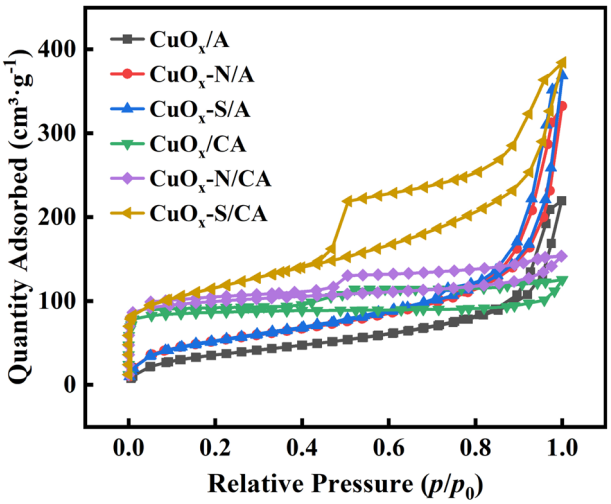

Fig. 6 Isothermal adsorption and desorption curves of nitrogen before and after carbonization of CuO_x/CA, CuO_x-N/CA, CuO_x-S/CA.

g^{-1}, respectively. This indicates that the loading of copper salts has blocked the pores of the cellulose aerogel, while the decomposition of copper salts works in synergy with the carbonization of cellulose to play a key role in the pore formation process.

3.2.2 XRD and Raman spectra. The XRD patterns of CuO_x/CA, CuO_x-N/CA, and CuO_x-S/CA are shown in Fig. 7(a). All three copper oxide/carbon composites exhibit five distinct diffraction peaks at 43.33°, 50.50°, 74.20°, 90.02°, and 95.30°, corresponding to the (2 0 0) plane of Cu_2O, the (1 1 2) and (3 1 1) planes of CuO, and the (1 3 1) plane of CuO, and the (3 2 2) plane of Cu_2O, respectively.[34] In addition, CuO_x-S/CA shows smaller diffraction peaks of CuS at 27.70°, 32.53°, and 46.00°, corresponding to the (1 0 1), (0 0 6), and (1 0 7) planes of CuS, indicating the coexistence of copper oxides and sulfides in CuO_x-S/CA.[35]

The Raman spectrum in Fig. 7(b) indicates that three samples have defect peak and graphite peak, illustrating the sp^3 disordered carbon structure and sp^2 graphite carbon structures

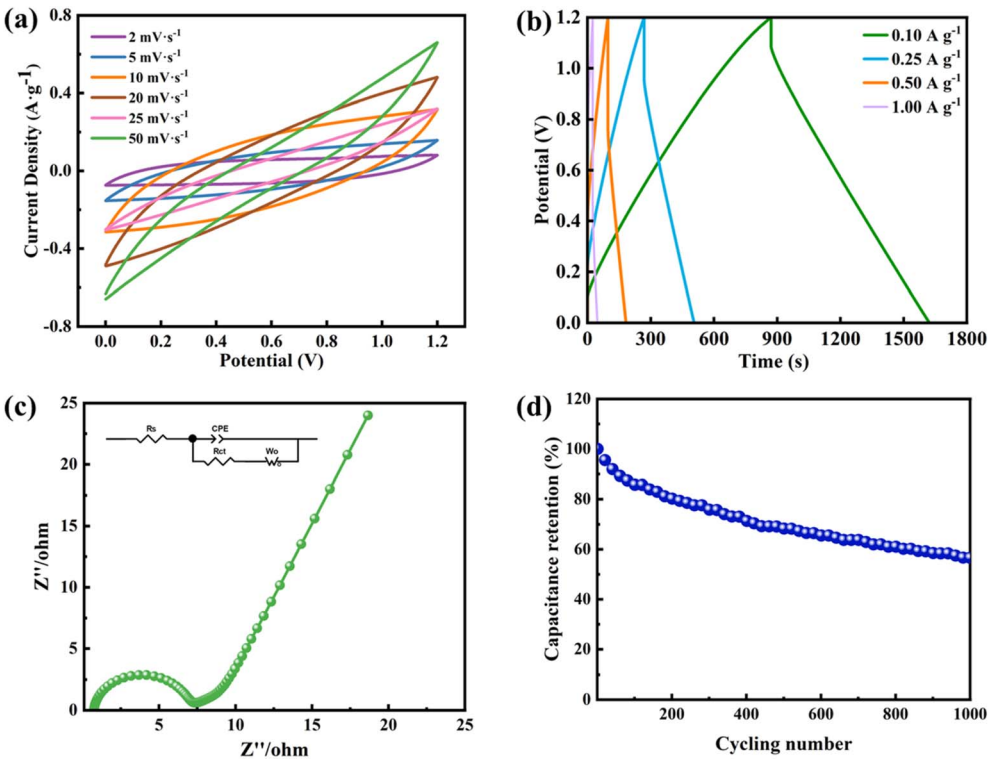

Fig. 5 Electrochemical properties of an asymmetric supercapacitor. (a) Cyclic voltammetry curves, (b) galvanostatic charge/discharge curve, (c) AC impedance spectrum, (d) cyclic performance diagram of 1.0 A g^{-1}.

© 2025 The Author(s). Published by the Royal Society of Chemistry

Open Access Article. Published on 03 March 2025. Downloaded on 6/14/2026 4:03:39 PM.
This article is licensed under a Creative Commons Attribution-NonCommercial 3.0 Unported Licence.

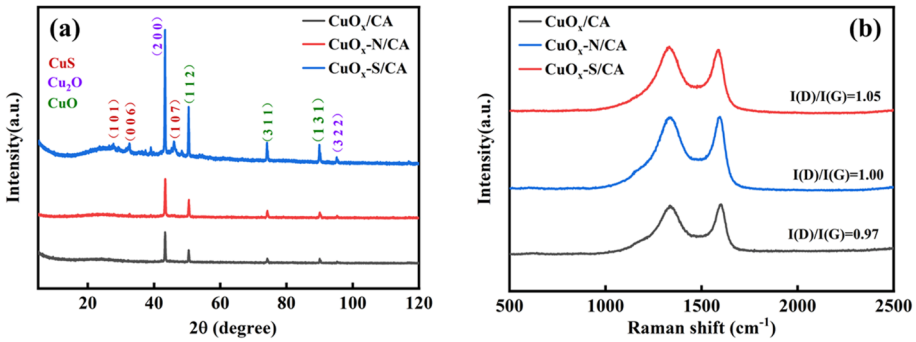

Fig. 7 The XRD patterns and Raman spectra of CuO$_x$/CA, CuO$_x$-N/CA and CuO$_x$-S/CA. (a): XRD patterns, (b) Raman spectra.

both exist in the material.[36,37] The I(D)/I(G) ratios for CuO$_x$/CA, CuO$_x$-N/CA, and CuO$_x$-S/CA are 0.97, 1.00, and 1.05, respectively, suggesting that the degree of disorder in CuO$_x$-S/CA is more pronounced and beneficial to its electrochemical performance. This result could be attributed to the fact that the atomic radius of sulfur is larger than that of carbon, and its doping can induce greater strain in the material, leading to the formation of more defect sites and increasing the degree of disorder.[38]

3.2.3 SEM and EDS. The micromorphologies of CuO$_x$/CA, CuO$_x$-N/CA, and CuO$_x$-S/CA are shown in Fig. 8(a)–(c), respectively. It can be observed that there are uniformly distributed spherical copper oxide particles in the three materials, and the pores of the carbon are more distinct in the samples of CuO$_x$-N/CA and CuO$_x$-S/CA. In the EDS results of Fig. 8(d)–(i), the overall uniform distribution of Cu element in these three materials indicates that this preparation method has achieved satisfactory dispersion of the copper oxides. Additionally, the presence of S can be found in CuO$_x$-S/CA, and the content of C, O, Cu and S based on the results of EDS in this composite are 92.0%, 0.8%, 6.8% and 0.4%, respectively.

3.2.4 XPS. XPS analysis was conducted on CuO$_x$/CA, CuO$_x$-N/CA, and CuO$_x$-S/CA to investigate the chemical states of the elements on the material surface. Fig. 9(a) shows the full XPS spectra of. In the full XPS spectra, characteristic peaks for Cu, C, and O are present in all samples. The C 1s spectrum in Fig. 9(b) shows characteristic peaks for C–C, C–O, and C=O bonds at 284.79 eV, 289.08 eV, and 291.36 eV, respectively, and a C–S characteristic peak can be observed at 285.72 eV.[39] As shown in Fig. 9(c), the O 1s spectrum can be divided into diffraction peaks for C–O, C=O, and Cu–O, corresponding to 532.36 eV, 533.78 eV, and 527.50 eV, respectively.[40] The fitting results of the

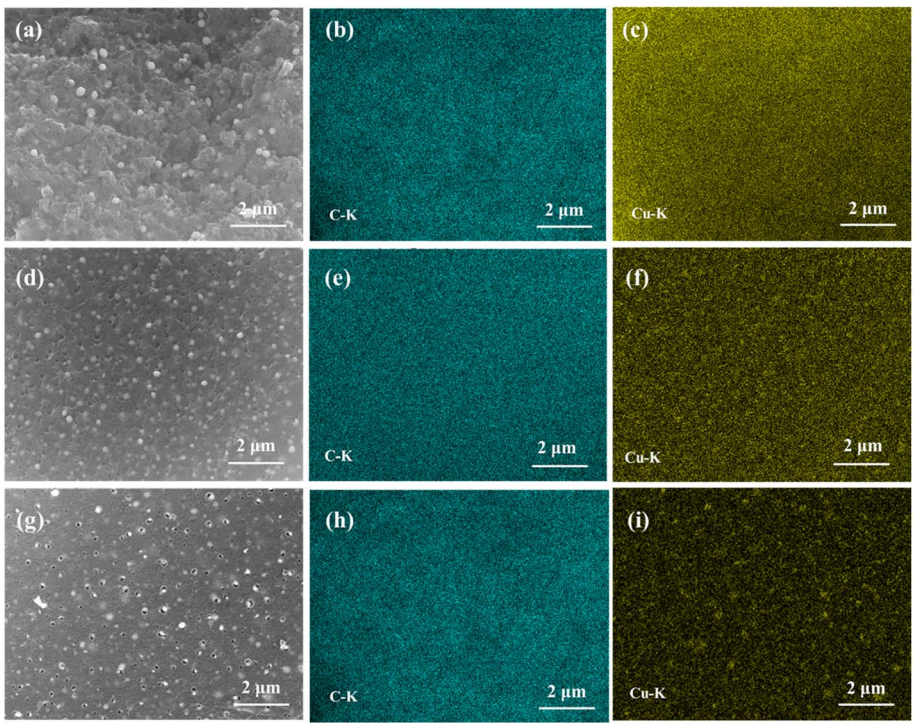

Fig. 8 The SEM and elemental maps of copper oxide/carbon composites. CuO$_x$/CA: (a) SEM, (b) C, (c) Cu, CuO$_x$-N/CA: (d) SEM, (e) C, (f) Cu, CuO$_x$-S/CA: (g) SEM, (h) C, (i) Cu.

Open Access Article. Published on 03 March 2025. Downloaded on 6/14/2026 4:03:39 PM.
This article is licensed under a Creative Commons Attribution-NonCommercial 3.0 Unported Licence.

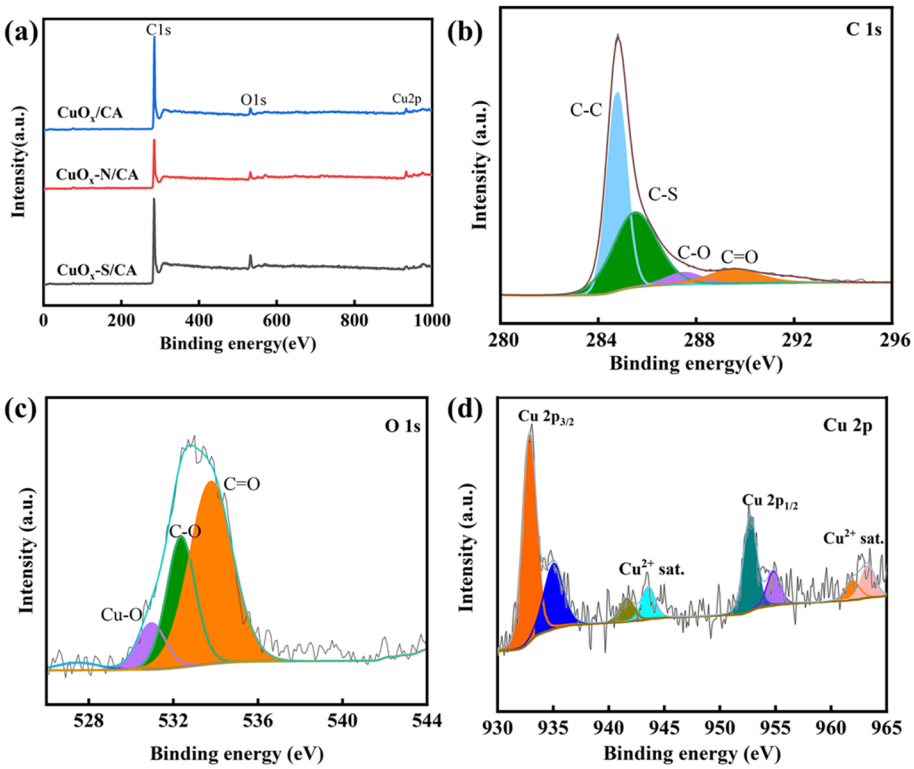

Fig. 9 XPS spectrum of CuO_x/CA, CuO_x-N/CA, CuO_x-S/CA. (a) Full-scan spectrum, (b)–(d) high-resolution spectra of C, O, Cu of CuO_x-S/CA.

high-resolution Cu 2p spectrum are shown in Fig. 9(d). Two distinct peaks can be observed at 932.80 eV and 953.08 eV, corresponding to the Cu $2p_{3/2}$ and Cu $2p_{1/2}$ peaks, respectively, which indicates the presence of copper in both +1 and +2 oxidation states.[41] In addition, the presence of satellite peaks at 943.58 eV and 963.18 eV also confirms the existence of Cu in the +2 oxidation state.[42]

4 Conclusion

The copper oxide/carbon composites, which have a high specific surface area and uniform dispersion, were prepared using cellulose aerogel loaded with copper acetate, copper nitrate, and copper sulfate as precursors, and the electrochemical performance of these materials was analyzed. At a current density 2 A g^{-1}, the mass-specific capacitance of CuO_x/CA, CuO_x-N/CA, and CuO_x-S/CA reached 254 F g^{-1}, 239 F g^{-1}, and 1001 F g^{-1}, respectively. Correspondingly, their energy densities were 33.3 W h kg^{-1}, 35.3 W h kg^{-1}, and 139.0 W h kg^{-1}, respectively. Asymmetric supercapacitors were assembled using CuO_x-S/CA as the positive electrode material, activated carbon as the negative electrode material, and 3.0 M KOH as the electrolyte. This device showed low resistance, with a mass-specific capacitance of 125 F g^{-1} at a current density of 0.1 A g^{-1}, and an energy density of 6.3 W h kg^{-1}. Among these copper oxide/carbon composites, the CuO_x-S/CA material demonstrated the highest mass-specific capacitance and energy density. This superior performance can be attributed to its largest specific surface area and the introduction of sulfur atoms, which introduces more carbon defects in the material and creates additional active sites for redox reactions, thereby enhancing the mass-specific capacitance and energy density.

Data availability

The data that support the findings of this study are available from the corresponding authors upon reasonable request.

Conflicts of interest

The authors have no competing conflict of interest.

Acknowledgements

This work was supported by the Natural Science Foundation of Sichuan, China (2022NSFSC0308).

References

1 A. Borenstein, O. Hanna, R. Attias, S. Luski, T. Brousseb and D. Aurbach, Carbon-based composite materials for supercapacitor electrodes: a review, *J. Mater. Chem. A*, 2017, **5**(25), 12653–12672.
2 T. Ramachandran, S. S. Sana, K. D. Kumar, Y. A. Kumar, H. H. Hegazy and S. C. Kim, Asymmetric supercapacitors: Unlocking the energy storage revolution, *J. Energy Storage*, 2023, **73**(C), 109096.

© 2025 The Author(s). Published by the Royal Society of Chemistry

Open Access Article. Published on 03 March 2025. Downloaded on 6/14/2026 4:03:39 PM. This article is licensed under a Creative Commons Attribution-NonCommercial 3.0 Unported Licence.

3 Y. Shao, M. F. El-Kady, J. Sun, Y. Li, Q. Zhang, M. Zhu, H. Wang, B. Dunn and R. B. Kaner, Design and mechanisms of asymmetric supercapacitors, *Chem. Rev.*, 2018, **118**(18), 9233–9280.

4 S. Reenu, L. Phor, A. Kumar and S. Chahal, Electrode materials for supercapacitors: A comprehensive review of advancements and performance, *J. Energy Storage*, 2024, (84), 110698.

5 L. L. Zhang and X. S. Zhao, Carbon-based materials as supercapacitor electrodes, *Chem. Soc. Rev.*, 2009, **38**(9), 2520–2531.

6 K. K. R. Reddygunta and B. D. Kumar, Biomass activated carbon composites and their potential in supercapacitor applications: current trends and future perspectives, *Energy Fuels*, 2024, **38**(12), 10560–10588.

7 Z. D. Pan, S. Yu, L. F. Wang, C. Li, F. Mei, N. Wang, S. Zhou, Y. Xiong, Z. Wang, Y. Wu, X. Liu, B. Fang and Y. Zhang, Recent advances in porous carbon materials as electrodes for supercapacitors, *Nanomaterials*, 2023, **13**(11), 1744.

8 M. D. Stoller, S. Park, Y. Zhu, J. An and R. S. Ruoff, Graphene-based ultracapacitors, *Nano Lett.*, 2008, **8**(10), 3498–3502.

9 Y. Yan, Y. X. Yin, S. Xin, Y. G. Guo and L. J. Wan, Ionothermal synthesis of sulfur-doped porous carbons hybridized with graphene as superior anode materials for lithium-ion batteries, *Chem. Commun.*, 2012, **48**(86), 10663–10665.

10 W. H. Shin, H. M. Jeong, B. G. Kim, J. K. Kang and J. W. Choi, Nitrogen-doped multiwall carbon nanotubes for lithium storage with extremely high capacity, *Nano Lett.*, 2012, **12**(5), 2283–2288.

11 R. Reit, J. Nguyen and W. J. Ready, Growth time performance dependence of vertically aligned carbon nanotube supercapacitors grown on aluminum substrates, *Electrochim. Acta*, 2013, **91**, 96–100.

12 H. Liu, T. Xu, Q. Liang, Q. Zhao, D. Zhao and C. Si, Compressible cellulose nanofibrils/reduced graphene oxide composite carbon aerogel for solid-state supercapacitor, *Adv. Compos. Hybrid Mater.*, 2022, **5**(2), 1168–1179.

13 J. Li, S. Chen, X. Zhu, X. She, T. Liu, H. Zhang, S. Komarneni, D. Yang and X. Yao, Toward aerogel electrodes of superior rate performance in supercapacitors through engineered hollow nanoparticles of $NiCo_2O_4$, *Adv. Sci.*, 2017, **4**(12), 1700345.

14 Y. W. Zhu, S. Murali, M. D. Stoller, K. J. Ganesh, W. Cai, P. J. Ferreira, A. Pirkle, R. M. Wallace, K. A. Cychosz, M. Thommes, D. Su, E. A. Stach and R. S. Ruoff, Carbon-based supercapacitors produced by activation of graphene, *Science*, 2011, **332**(6037), 1537–1541.

15 G. Wang, R. Liang, L. Liu and B. Zhong, Improving the specific capacitance of carbon nanotubes-based supercapacitors by combining introducing functional groups on carbon nanotubes with using redox-active electrolyte, *Electrochim. Acta*, 2014, **115**, 183–188.

16 E. Lei, W. Gan, J. Sun, Z. Wu, C. Ma, W. Li and S. Liu, High-performance supercapacitor device with ultrathick electrodes fabricated from all-cellulose-based carbon aerogel, *Energy Fuels*, 2021, **35**(9), 8295–8302.

17 I. Shaheen, I. Hussain, T. Zahra, M. S. Javed, S. S. A. Shah, K. Khan, M. B. Hanif, M. A. Assiri, Z. Said, W. U. Arifeen, B. Akkinepally and K. Zhang, Recent advancements in metal oxides for energy storage materials: Design, classification, and electrodes configuration of supercapacitor, *J. Energy Storage*, 2023, **72**(E), 108719.

18 A. K. Lichchhavi and P. M. Shirage, A review on synergy of transition metal oxide nanostructured materials: Effective and coherent choice for supercapacitor electrodes, *J. Energy Storage*, 2022, **55**(C), 105692.

19 F. Jamal, A. Rafique, S. Moeen, J. Haider, W. Nabgan, A. Haider, M. Imran, G. Nazir, M. Alhassan, M. Ikram, Q. Khan, G. Ali, M. Khan, W. Ahmad and M. Maqbool, Review of metal sulfide nanostructures and their applications, *ACS Appl. Nano Mater.*, 2023, **6**(9), 7077–7106.

20 E. H. Bao, J. L. Sun, Y. F. Liu, X. Ren, X. Liu, C. Xu and H. Chen, Facile preparation of SnS_2 nanoflowers and nanoplates for the application of high-performance hybrid supercapacitor, *Int. J. Hydrogen Energy*, 2022, **47**(92), 39204–39214.

21 W. Wang, D. Chen, F. Li, X. Xiao and Q. Xu, Metal-organic-framework-based materials as platforms for energy applications, *Chem*, 2024, **10**(1), 86–133.

22 C. Xiong, Y. Zhang, C. Zheng, Y. Yin, Q. Xiong, M. Zhao and B. Wang, Fabrication of metal-organic framework@cellulose nanofibers/reduced graphene oxide-Vitrimer composite electrode materials with shape memory for supercapacitors, *Electrochim. Acta*, 2024, **493**, 144373.

23 H. R. Naderi, P. Norouzi and M. R. Ganjali, Electrochemical study of a novel high erformance supercapacitor based on MnO_2/nitrogen-doped graphene nanocomposite, *Appl. Surf. Sci.*, 2016, **366**, 552–560.

24 Y. Cui, L. Zhao, H. Pan, P. Hong, C. Zhao, J. Wang, L. Meng, H. Yu, B. Zhao, X. Che, J. Yang, X. Gao and X. Xu, ZIF-9 derived rGO/$NiCo_2S_4$ composite as the electrode materials for high performance asymmetric supercapacitor, *Microchem. J.*, 2023, **190**, 108718.

25 P. Wen, P. Gong, J. Sun, J. Wang and S. Yang, Design and synthesis of Ni-MOF/CNT composites and rGO/carbon nitride composites for an asymmetric supercapacitor with high energy and power density, *J. Mater. Chem. A*, 2015, **3**(26), 13874–13883.

26 M. P. Chavhan, M. Khandelwal, S. Arya, T. Das, A. Singh and O. Ghodbane, A review of nanocomposites/hybrids made from biomass-derived carbons for electrochemical capacitors, *Chem. Eng. J.*, 2024, **500**(15), 157267.

27 C. Xiong, C. Zheng, Z. Zhang, Q. Xiong, Q. Zhou, D. Li, M. Shen and Y. Ni, Polyaniline@cellulose nanofibers multifunctional composite material for supercapacitors, electromagnetic interference shielding and sensing, *J. Mater.*, 2025, **11**(1), 100841.

28 C. Chen and L. Hu, Nanocellulose toward advanced energy storage devices: structure and electrochemistry, *Acc. Chem. Res.*, 2018, **51**(12), 3154–3165.

29 K. I. Nargatti, A. R. Subhedar and A. Dufresne, Nanocellulose-based aerogel electrodes for

Open Access Article. Published on 03 March 2025. Downloaded on 6/14/2026 4:03:39 PM.
This article is licensed under a Creative Commons Attribution-NonCommercial 3.0 Unported Licence.

supercapacitors: A review, *Carbohydr. Polym.*, 2022, **297**, 120039.

30 C. M. Walters, G. K. Matharu, W. Y. Hamad, E. Lizundia and M. J. MacLachlan, Chiral nematic cellulose nanocrystal/germania and carbon/germania composite aerogels as supercapacitor materials, *Chem. Mater.*, 2021, **33**(13), 5197–5209.

31 L. J. Andrew, E. R. Gillman, C. M. Walters, E. Lizundia and M. J. MacLachlan, Multi-responsive supercapacitors from chiral nematic cellulose nanocrystal-based activated carbon aerogels, *Small*, 2023, **19**, 2301947.

32 I. V. Esarev, D. V. Agafonov, Y. V. Surovikin, S. N. Nesov and A. V. Lavrenov, On the causes of non-linearity of galvanostatic charge curves of electrical double layer capacitors, *Electrochim. Acta*, 2021, **390**, 138896.

33 S. Teng, G. Siegel, M. C. Prestgard, W. Wang and A. Tiwari, Synthesis and characterization of copper-infiltrated carbonized wood monoliths for supercapacitor electrodes, *Electrochim. Acta*, 2015, **161**, 343–350.

34 P. K. Singh, A. K. Das, G. Hatui and G. C. Nayak, Shape controlled green synthesis of CuO nanoparticles through ultrasonic assisted electrochemical discharge process and its application for supercapacitor, *Mater. Chem. Phys.*, 2017, **198**, 16–34.

35 U. Shamraiz, R. A. Hussain and A. Badshah, Fabrication and applications of copper sulfide (CuS) nanostructures, *J. Solid State Chem.*, 2016, **238**, 25–40.

36 L. Qie, W. Chen, Z. Wang, Q. Shao, X. Li, L. Yuan, X. Hu, W. Zhang and Y. Huang, Nitrogen-doped porous carbon nanofiber webs as anodes for lithium ion batteries with a superhigh capacity and rate capability, *Adv. Mater.*, 2012, **24**(15), 2047–2050.

37 J. Ding, H. Wang, Z. Li, A. Kohandehghan, K. Cui, Z. Xu, B. Zahiri, X. Tan, E. M. Lotfabad and B. C. Olsen, David Mitlin, Carbon nanosheet frameworks derived from peat moss as high performance sodium ion battery anodes, *ACS Nano*, 2013, **7**(12), 11004–11015.

38 R. Bowling, R. T. Packard and R. L. McCreery, Mechanism of electrochemical activation of carbon electrodes role of graphite lattice defects, *Langmuir*, 1989, **5**, 683–688.

39 X. Hou, Y. Zhang, Q. Dong, Y. Hong, Y. Liu, W. Wang, J. Shao, W. Si and X. Dong, Metal organic framework derived core–shell structured Co_9S_8@N-C@MoS_2 nanocubes for supercapacitor, *ACS Appl. Energy Mater.*, 2018, **1**(07), 3513–3520.

40 S. Lei, L. Chen, W. Zhou, P. Deng, Y. Liu, L. Fei, W. Lu, Y. Xiao and B. Cheng, Show more Tetra-heteroatom self-doped carbon nanosheets derived from silkworm excrement for high-performance supercapacitors, *J. Power Sources*, 2018, **379**, 74–83.

41 H. Jiang, X. Yan, J. Miao, M. You, Y. Zhu, J. Pan, L. Wang and X. Cheng, Super-conductive silver nanoparticles functioned three-dimensional Cu_xO foams as a high-pseudocapacitive electrode for flexible asymmetric supercapacitors, *J. Mater.*, 2021, **7**(1), 156–165.

42 H. Jiang, X. Yan, J. Miao, M. You, Y. Zhu, J. Pan and L. Wang, Facile synthesis of microsphere copper cobalt carbonate hydroxides electrode for asymmetric supercapacitor, *Electrochim. Acta*, 2016, **188**, 898–908.

© 2025 The Author(s). Published by the Royal Society of Chemistry